Analysis for the Progressive Failure Response of Textile Composite Fuselage Frames

Final Report — Summary of Research

Eric R. Johnson
Principal Investigator

Performance Period: 10 June 2000 to 09 June 2001

NASA Grant NAG-1-2309

Aerospace and Ocean Engineering Department
Virginia Polytechnic Institute and State University
Blacksburg, Virginia 24061-0203

February 19, 2002

Technical Officer: Dr. Richard L. Boitnott, Mail Stop 495
National Aeronautics and Space Administration
Langley Research Center
Hampton, Virginia 23681-2199

Introduction

A part of aviation accident mitigation is a crash worthy airframe structure, and an important measure of merit for a crash worthy structure is the amount of kinetic energy that can be absorbed in the crush of the structure. Prediction of the energy absorbed from finite element analyses requires modeling the progressive failure sequence. Progressive failure modes may include material degradation, fracture and crack growth, and buckling and collapse. The design of crash worthy airframe components will benefit from progressive failure analyses that have been validated by tests. The subject of this research is the development of a progressive failure analysis for textile composite, circumferential fuselage frames subjected to a quasi-static, crash-type load. The test data for these frames are reported in Ref. 1, and these data, along with stub column test data, are to be used to develop and to validate methods for the progressive failure response.

Circumferential Frame Specimens and Tests

The structural components tested in Ref. 1 were the size of a typical circumferential fuselage frame for a wide body commercial transport aircraft with a nominal inside radius of 118 inches and a radial depth of 4.8 inches. The frame segments are 48° circular arcs with an asymmetrical cross section in the shape of the letter *J*. A detailed illustration of a frame and its cross section with dimensions given parametrically is shown in Fig. 1. Measurements of the three frames used in Ref. 1, which are denoted as A, B, and C, are listed in Table 1.

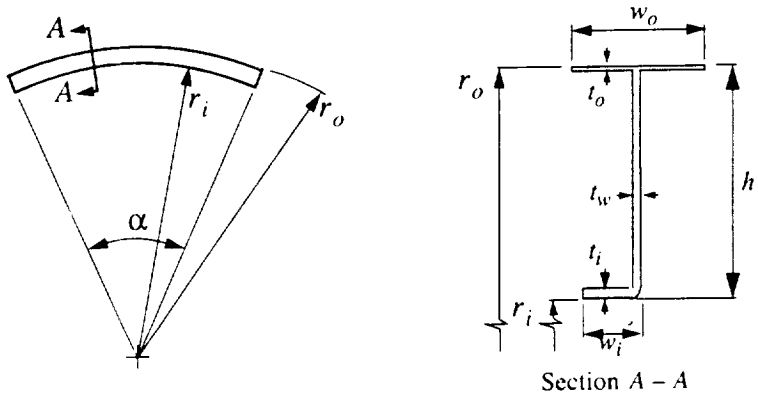

Fig. 1 J-section fuselage frame

Table 1. Braided composite frame measurements (Ref. 1).

Dimension as shown in Fig. 1	Frame		
	A	B	C
w_i, in.	1.24	1.25	1.27
w_o, in.	2.78	2.77	2.80
t_i, in.	0.198	0.204	0.202
t_o, in.	0.0892	0.0885	0.0920
t_w, in.	0.162	0.159	0.172
h, in.	4.78	4.80	4.81
r_i, in.	117.25	117.85	118.92
r_o, in.	122.03	122.65	123.73
α, degrees	48.18	47.21	47.46

The frames were fabricated from 2X2 2-D triaxial braided textile composite preforms coupled with the resin transfer molding process using 3M PR500 epoxy resin. The architecture of the preforms is $[0°_{18k}/\pm 64°_{6k}]$ 39.7% axial, and the yarns are made of AS4 graphite fibers. Material property data are listed in Table 2. The number of layers in the web and inner flange is the same, but, as can be seen from the thicknesses listed in Table 1, the thickness of the radially inboard flange is greater than the thickness of the web. Hence, because of the manufacturing process there is a reduced fiber volume fraction in the radially inner flange. Reduction of the fiber volume fraction is due to an increase in volume of resin in the inner flange. The fiber volume fraction in the inner flange, $(V_f)_i$, was approximated by $(V_f)_i = (t_w V_{fw})/t_i = 0.4307$. According to Naik[2], the relationship between the fiber volume fraction and the moduli are approximately linear. These data from Ref. 2 are for a material with an architecture of $[0°_{18k}/\pm 67.4°_{6k}]$, yarn packing density of 0.75, and axial yarn spacing 5.32 mm. Other than the 3.4° difference in the braider angle this architecture matches that of the frames. Using slopes measured from the plots in Ref. 3, the reduced moduli for the inner flange are $E_{11} = 5.83\times10^6$ psi and $E_{22} = 5.09\times10^6$ psi. The variation in the shear moduli with fiber volume fraction is negligible, so it and other property data for the inner flange are as listed for the web and outer flange in Table 2.

Table 2. Tri-axial braid properties for V_f = 55.26%

Properties	TEXCAD[3]	Tension Tests[5]
Axial Modulus (E_{11},psi)	7.06×10^6	7.09×10^6
Transverse Modulus (E_{22},psi)	6.59×10^6	N/A
Through Thickness Modulus (E_{33},psi)	1.53×10^6	N/A
Poisson's Ratio (ν_{12})	0.231	0.26
Poisson's Ratio (ν_{13})	0.216	N/A
Poisson's Ratio (ν_{23})	0.298	N/A
In Plane Shear Modulus (G_{12},psi)	1.91×10^6	N/A
Transverse Shear Modulus (G_{13},psi)	0.601×10^6	N/A
Transverse Shear Modulus (G_{23}, psi)	0.645×10^6	N/A
Tensile Failure Strain ($\varepsilon_1^{f\,T}$, $\mu\varepsilon$)	14071	10588
Compression Failure Strain (ε_1^{c}, $\mu\varepsilon$)	10108	N/A

A sketch of the frame mounted in a universal testing machine is shown Fig. 2. The structural testing consisted of mounting frames B and C vertically, convex side up, in a universal testing machine and subjecting them to a slowly applied, radially inward displacement at their apex.

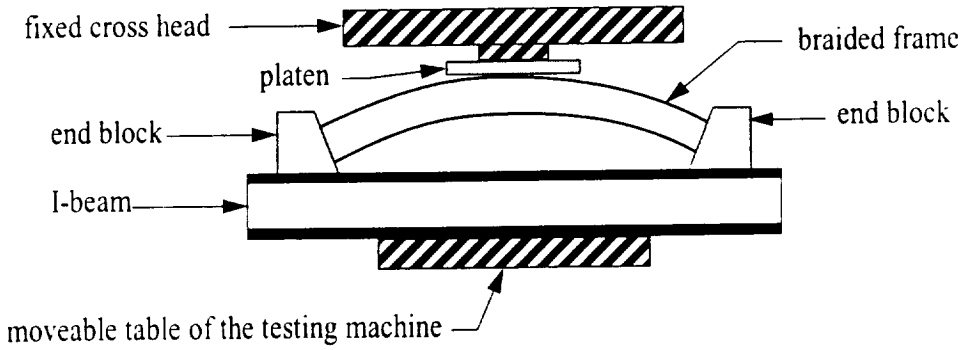

Fig. 2 Sketch of the frame test apparatus

Similar load-deflection curves were exhibited in the quasi-static tests of frames B and C. In addition to in-plane bending and circumferential compression, these asymmetric *J*-section frames

exhibit out-of-plane bending and torsion. The largest circumferential strain magnitude was compressive and occurred in the outer flange at the apex. A compressive hoop strain of approximately one-half this maximum value occurred in the inner flange at the ends of the frame. The largest circumferential tensile strains are much less than the largest compressive strain magnitudes. The maximum compressive strain recorded at the first major failure event is about 4000 με which is substantially less than the material ultimate compression strain of 10,108 με predicted by TEXCAD[3] computer program for this material system.

Stub Column Tests

Stub column tests are used to determine the tangent modulus of steel columns[4], since the critical load for column buckling is based on the tangent modulus theory. The tangent modulus is the slope of the compressive stress-strain curve obtained from the stub column test data. Stub column stress-strain data differ from the material coupon tests because of the presence of residual stresses in the former that are not present in the latter. The fabrication process for steel columns involves heating and cooling, and this thermal cycle leads to residual stresses in the steel member. The stub column test, then, can account for the residual stresses due to fabrication whereas the material coupon test is free of residual stresses.

Similar to the steel stub column tests, the goal of performing the stub column tests on the composite *J*-section is to obtain compressive strength data that accounts for fabrication features unique to the cross section that are not present in coupon testing. For example, in the test of Frame C it was noticed that a circumferential ligament of material separated from the junction of the web and outer flange of the frame in contact with the upper platen. See the photograph on page 104 of Ref. 5. It appears that in the fabrication of the frame that material was inserted along the circumference in the void created by splitting the fabric in the web to form the flanges. Since the largest compressive strains in the frame occur where the frame contacts the upper platen, it seems reasonable that this fabrication feature at the junction would account for a lower compressive strength of the section than that reported for the material. Consequently, the purpose of the stub column tests is to quantify the effect of the junction construction, and any other fabrication anomalies, on the compressive failure response of the section.

Preliminary tests

These first tests involved unsupported 2-inch-long columns cut from Frame B that were loaded in flat-end compression until failure. Loads and displacements were recorded in a series of four tests with the fourth test specimen fitted with back to back axial strain gages at locations on the web and inner flange. Because the ends of the stub columns were not supported in end fixtures, the failed specimens exhibited end brooming. End brooming appeared to initiate specimen failure from the inner radial flange. Finite element analyses of these tests were performed using the ABAQUS software package[6]. A branched shell model of the stub column specimens was constructed using the shell element S4R5 in the ABAQUS library of elements. A model geometry and finite element mesh were selected that lead to converged response results. Then the longitudinal modulus of the material was adjusted slightly such that the analysis matched initial load end-shortening data from the test. The buckling load calculated from the finite element analysis was

within 2% of the maximum load attained in the test. The correlation of the predicted buckling load and the failure load from the test meant that the specimen may have buckled before material failure occurred.

Second series of tests

The second series of tests were not completed during the performance period of this report. However, the design of the test apparatus and instrumentation was determined, and the machining of the fixtures was completed. From the results of the preliminary tests, the ends of the stub columns in this second series are supported in end fixtures to avoid the end brooming observed in the preliminary tests. ABAQUS predictions of the buckling loads along with material compressive failure predictions with TEXCAD were used to determine lengths for the test specimens that would either buckle first or exceed the compressive strength of the textile material first. To achieve a material compressive failure prior to buckling, a stub column length of 1.5 inches was determined. To study the local buckling of the outer flange, 4- and 6-inch stub column heights were chosen. A total of nine specimens, three of each length, were cut from Frame A and C. Stub column specimens 1 through 6 were cut from frame C, and 7 through 9 were cut from frame A. Frame C was tested May 21, 1999 at the Impact Dynamics Research Facility, and the specimens were cut from sections of the frame that had no visible damage. Frame A was not tested in Ref. 1. and was used for material coupons. The stub columns were cut 2.5-inches longer than the gage lengths to accommodate one inch of potting material on each end, as well as for machining the specimens flat and parallel.

The potting material consisted of 934 Hysol epoxy with glass beads. Glass beads were added approximately 20% by weight. This made the mixture 3 parts epoxy, 1 part hardener, and 1 part glass beads. The mold used for the potting material consisted of two parts, the first part was a 6 x 4 inch steel box beam with 0.25 inch wall thickness cut into 1 inch lengths. The second part was a thin piece of silicone rubber cut to match the interior opening of the box beam. The steel box beam is lined up over the cut out in the silicone rubber, and the potting compound is poured into the mold. The specimen is then pushed into the mixture and aligned so that the mid-point cross section is approximately parallel to the testing surface. When the base is cured, the process is repeated for the opposite end of the specimen. The gage lengths of the specimens are nominally 1.5, 4, and 6 inches.

Electrical resistance strain gages were bonded to the test specimens parallel to the load axis. Back-to-back axial strain gages on the 1.5 and 4-inch specimens were located on the outer flange edges at the mid-height to measure the bending strains in pre- and post-buckling. Two different buckling modes for the 6-inch specimen were determined from two different ABAQUS models. When the stub column was modeled as the six inches long with clamped end conditions, the buckling modes predicted in the outer flanges are two half waves, with the mode in one flange a 180 degrees out of phase with respect to the opposite flange. If the stub column is modeled to include the extra column length and the potting simulated by boundary conditions constraining the lateral displacements of the nodes, the buckling shape of the outer flange consists of three half waves. The outer flange on the opposite side has this same buckling mode but 180 degrees out of phase. Back-to-back strain gage locations were determined such that either of these buckling modes would be evident from the strain gage responses.

Finite element models

The finite element models were constructed with element type S4R5 which has 4 nodes with 5 degrees of freedom each. Individual nodes may contain 6 degrees of freedom if 6 degrees of freedom are specified or the node is in contact with another node containing 6 degrees of freedom. The S4R5 element is a doubly curved thin walled shell with reduced integration and an optional hourglass control. The finite element models of the stub columns included the frame curvature, 3D orthotropic material properties contained in a single homogeneous layer, and reduced moduli for the inner flange. The measured thickness of the inner flange is larger than the thickness of the web, but the inner flange and web have the same number of layers. The larger thickness of the inner flange means this flange has excess resin relative to the web, and hence a lower fiber volume fraction. The flanges and web are modeled as a single orthotropic layer by specifying the nine independent engineering material properties. Element S4R5 uses numerical integration through the thickness of the shell to compute the section properties.

Frame *B* Finite Element Model

Finite element models of frame B^1 were developed in ABAQUS using the dimensions listed in Table 1, material property data for the web and outer flange listed in Table 2, reduced Young moduli for the inner flange as discussed in previously, and using shell element S4R5. One model, the coarse mesh model, had 999 nodes and 870 elements with an average element dimension of 1.2 in. X. 1.0 in. A second model with a finer mesh containing 3757 nodes and 3530 elements with average element dimensions of 0.6 in. X. 0.5 in. was also considered. Both meshes gave the same initial stiffness of the frame. However, the finer mesh was used to determine the results presented below, since failure is associated with localized deformation. Clamped boundary conditions were prescribed in the analyses to simulated the frame mounted in the end blocks.

Two mid-span loading schemes were tried to simulate the contact of the platen with the frame. Refer to the test configuration shown in Fig. 2 to see the location of the platen relative to the frame. The first scheme was a line load specified at midspan. Along the line of nodes across the width of the top flange at midspan, the displacements in the direction out of the plane of the frame were specified to be zero, and the displacements in the radial inward direction were specified to be a non-zero value. The second scheme was a contact algorithm available in ABAQUS. A rigid plane parallel to the platen was displaced in the downward direction into the outer flange of the frame.

Results from three finite element models were studied: A linear elastic analysis with line loading, a geometrically nonlinear analysis with line loading, and a geometrically nonlinear analysis with contact loading. The nonlinear analyses use Newton s method, and the ABAQUS software issues warnings messages when the eigenvalues of the tangent stiffness matrix at an equilibrium state are negative. As the load is increased along the equilibrium path in the load-deflection space, the first equilibrium state encountered along the path where a negative eigenvalue occurs is an approximation of the critical state. The critical state divides stable and unstable equilibrium states along the equilibrium path. The initial structural stiffness of all three finite element analyses were essentially the same as the initial stiffness from the test data.

However, the linear analysis was not capable of predicting the softening response exhibited by the test data. Both geometrically nonlinear analyses soften with increasing load, but the nonlinear analysis with the contact algorithm more closely correlated best with the test data. A quantitative comparison between the analyses and test is given in Table 3. The first major failure event in the test occurred at a displacement of 0.4782 inches and the corresponding force was 5,791.6 lbs. The force from the linear analysis at this displacement is 29.4% larger than the test. The displacements and corresponding forces at the critical equilibrium states from the nonlinear analyses are listed in Table 3 for comparison to the test. As is shown by the data in the table, the nonlinear analysis with contact more closely correlates with the first major failure event in the test.

Table 3. Responses from several analyses compared to the test of frame *B*

Analysis type	Specified midspan loading[a]		Midspan reaction force (lbs)	% Discrepancy with respect to test[b]	
	Type	Displacement (in.)		Displacement	Force
Linear	Line	0.4782	7498.5	0.0	29.4
Nonlinear	Line	0.4103	4345.4	-14.2	-24.9
Nonlinear	Contact	0.4042	5604.3	-15.5	-3.2

a. The displacement out of the plane of the frame is specified to be zero, and the value of the specified radially inward displacement is listed in column three.

b. The first major failure event occurred at a displacement of 0.4782 inches and at a midspan reaction force of 5791.6 lbs.

References

[1]Pérez, José G., Richard L. Boitnott, and Eric R. Johnson, "Tests of Braided Composite Fuselage Frames Under Radial Inward Load," *The 41st AIAA/ASME/ASCE/AHS/A SC Structures, Structural Dynamics, and Materials Conference and Exhibit*, (Atlanta Georgia, April 3-6, 2000), Compact Disk, American Institute of Aeronautics and Astronautics, Reston, VA, 2000, (AIAA Paper No. 2000-1547)

[2]Naik, Rajiv A., "Analysis of Woven and Braided Fabric Reinforced Composites," NASA Contractor Report 194930, June, 1994.

[3]Naik, R. A., "TEXCAD - Textile Composite Analysis for Design: Version 1.0 User's Manual", NASA CR-4639, National Aeronautics and Space Administration, Hampton, Virginia, 1994.

[4]Chen, W.F., and Lui, E.M., **Structural Stability**, Elsevier Science Publishing Co., Inc., New York, NY, 1987, pp.111-114,

[5]Pérez, José G., "Energy Absorption and Progressive Failure Response of Composite Fuselage Frames," Master of Science Thesis in Aerospace Engineering, Virginia Polytechnic Institute and State University, Blacksburg, VA 24061, July 1999.

[6]ABAQUS/Standard, Hibbitt, Karlsson, & Sorensen, Inc., 1080 Main St., Pawtucket, Rhode Island, 2001.

Student Supported by the Grant

Daniel C. Hart, Master of Science in Aerospace Engineering, Expected June, 2002.